Fluid–structure partitioned procedures based on Robin transmission conditions

Santiago Badia [a,*], Fabio Nobile [b], Christian Vergara [b,c]

[a] CIMNE, Universitat Politècnica de Catalunya, Jordi Girona 1-3, Edifici C1, 08034 Barcelona, Spain
[b] MOX – Dipartimento di Matematica "F. Brioschi" – Politecnico di Milano, Piazza Leonardo da Vinci 32, 20133 Milano, Italy
[c] Department of Information Technology and Mathematical Methods, Università degli Studi di Bergamo, viale Marconi 5, 24044 Dalmine (BG), Italy

Abstract

In this article we design new partitioned procedures for fluid–structure interaction problems, based on Robin-type transmission conditions. The choice of the coefficient in the Robin conditions is justified via simplified models. The strategy is effective whenever an incompressible fluid interacts with a relatively thin membrane, as in hemodynamics applications. We analyze theoretically the new iterative procedures on a model problem, which represents a simplified blood-vessel system. In particular, the Robin–Neumann scheme exhibits enhanced convergence properties with respect to the existing partitioned procedures. The theoretical results are checked using numerical experimentation.
© 2008 Elsevier Inc. All rights reserved.

Keywords: Fluid–structure interaction; Partitioned procedures; Transmission conditions; Robin boundary conditions; Added-mass effect; Hemodynamics

1. Introduction

In the last three decades, there has been an increasing interest in the simulation of fluid–structure interaction (FSI) problems that appear in several engineering and life science applications. We consider in this work the situation of an incompressible Newtonian fluid interacting with a relatively thin structure. Such situation appears for instance in hemodynamics applications when studying the interaction between blood and arterial wall. The numerical approximation of this type of heterogeneous systems is challenging. They are coupled and highly nonlinear problems with the following peculiarities:

---

* Corresponding author. Present address: Applied Mathematics and Applications, MS-1320, Sandia National Laboratories, Albuquerque, NM 87185-1320, United States.
    E-mail addresses: sbadia@cimne.upc.edu, sibadia@sandia.gov (S. Badia), fabio.nobile@polimi.it (F. Nobile), christian.vergara@polimi.it (C. Vergara).

(1) The position of the fluid–structure interface is an unknown of the coupled problem. It introduces a geo-
    metrical nonlinearity.
(2) The convective term of the fluid problem is nonlinear and, in case of using an ALE formulation (intro-
    duced in Section 2), also depends on the velocity of the fluid domain.
(3) The fluid and structure subproblems are coupled through transmission conditions which state the con-
    tinuity of velocity and normal stresses on the fluid–structure interface.

In this paper, we focus on algorithms based on subsequent solutions of fluid and structure sub-problems
(*partitioned procedures*). Every sub-problem is solved separately, allowing the reuse of existing codes/methods
(modularity). This is the main reason why partitioned procedures are so popular, see, e.g, [17,2,15,11,13].

In order to enforce continuity of velocity and normal stresses at the interface (condition (3)) one could con-
sider loosely coupled strategies, which solve the fluid and the structure only once (or just few times) per time
step and do not satisfy exactly the coupling transmission conditions. As a consequence, the work exchanged
between the two sub-problems is not perfectly balanced and this may induce instabilities in the numerical
scheme. For example, it was shown in [3] (see also [10]) that an explicit coupling is unstable in those applica-
tions where the added mass effect is important, as in hemodynamics. Alternatively, one can treat implicitly
(strongly) the coupling conditions at each time step, obtaining the solution of the fully coupled, monolithic
system of nonlinear equations. Several strategies have been proposed for the treatment of the nonlinearity.
In particular, one could consider Picard or Newton iterations over the nonlinear FSI system, to handle both
nonlinearities (1) and (2) (*implicit* strategy, see, e.g. [15,8]), or treat the interface position and the convective
term in an explicit way by extrapolation from previous time steps (*semi-implicit* algorithm, see, e.g. [7,16,1]). In
this way, no iterations are needed within each time step.

Whatever strategy is adopted, a sequence of linearized FSI problems (implicitly coupled through condition
(3)) has to be solved. Each of these problems can then be solved in a partitioned way via sub-iterations
between the fluid and structure sub-problems until convergence. Several iterative procedures have been inves-
tigated so far, see e.g. [20,5,13]. In all these approaches, the work exchanged between the two sub-problems is
perfectly balanced in each time step and the numerical scheme is stable. The price to pay is a relatively large
number of sub-iterations, particularly in those cases where the added mass is important. Up to now, the com-
putational cost remains extremely high.

The need to reduce the computational cost for those fluid–structure simulations where it is necessary to
treat implicitly the transmission conditions has motivated this work. In particular, we start from the Dirich-
let–Neumann (DN) partitioned procedure, in which the fluid problem is solved with a Dirichlet boundary con-
dition at the interface (the structure velocity at the previous sub-iteration) and the structure with a Neumann
boundary condition at the interface (the fluid normal stress just computed). This is the standard nomenclature
for partitioned procedures: the first kind of transmission conditions refers to the fluid sub-problem while the
second one refers to the structure sub-problem. This scheme is very easy to implement, yet, as shown in [3], it
often needs a large relaxation to converge and a quite high number of iterations when fluid and structure den-
sities are comparable.

This paper proposes new partitioned procedures based on Robin transmission conditions (linear combina-
tions of the Dirichlet and Neumann transmission conditions), applicable to those FSI problems where the
fluid and the structure have the same spatial dimension (say $d = 2, 3$). We introduce the general Robin–Robin
algorithm, which generates a whole family of partitioned procedures that includes the classical DN and other
new algorithms, such as the Robin–Dirichlet (RD), the Robin–Neumann (RN), the Dirichlet–Robin (DR) and
the Neumann–Robin (NR) schemes. At the algebraic level, all these algorithms can be interpreted as suitable
block Gauss–Seidel iterations on the monolythic FSI system.

The use of Robin transmission conditions is motivated by introducing simplified models for the fluid and
the structure (see [3,16]). In particular, in [16] a simple membrane model for a thin $(d-1)$-dimensional struc-
ture has been derived, under the assumption of normal displacements. It was shown that this model can be
embedded into the fluid problem leading to a Robin boundary condition. Hence, the original FSI problem
is reduced to a single fluid problem. A similar approach was previously proposed in [9] for a fixed fluid geom-
etry. For FSI problems in which the structure is d-dimensional, the previous considerations motivate the con-
struction of iterative procedures based on Robin transmission conditions applied to the fluid sub-problem.

The simplified model introduced in [16] also provides an estimate for the coefficient appearing in the Robin condition.

On the other hand, in [3] a simplified fluid model was considered, based on the assumption of inviscid fluid. It was shown that this model can be embedded into a $(d - 1)$-dimensional structure equation, by introducing a suitable "added mass" operator. In this work we consider the case of a d dimensional structure and show that this embedding procedure leads to a generalized Robin boundary condition. Upon approximating the added-mass operator with a multiple of the identity operator, the previous condition reduces to a "standard" Robin condition. This motivates the construction of iterative procedures based on Robin transmission conditions applied to the structure sub-problem, as well. Again, the simplified model introduced in [3] also provides an estimate for the coefficient appearing in the Robin condition.

We study the convergence of the RD and RN strategies on the model FSI problem proposed in [3] and extend the results given in [3] for the DN scheme. In particular, we provide the range of the relaxation parameter for which convergence is guaranteed. This theoretical analysis allows us to compare the efficiency of the different schemes and to understand the dependence of the convergence on different physical and numerical parameters. Our results indicate that, unlike the DN strategy, the RN scheme converges always without relaxation and independently of the added-mass effect.

Our preliminary numerical results presented in Section 6 show that the Robin–Neumann scheme features excellent convergence properties in comparison to the classical Dirichlet–Neumann approach. Moreover, the results confirm that convergence is almost independent of the added-mass effect. For these reasons we propose the Robin–Neumann scheme as a valid alternative to the Dirichlet–Neumann scheme for problems where the added-mass effect is significant. Among the other schemes, the Robin–Robin algorithm features even better convergence properties provided that the coefficient appearing in the Robin condition for the structure is properly chosen; the Dirichlet–Robin scheme features the same properties of the DN, while the Robin–Dirichlet and the Neumann–Robin scheme are very slow.

The outline of the paper is as follows. In Section 2 we introduce the fluid–structure interaction problem at the continuous level. In Section 2.1 we provide a suitable time discretization of the problem. In Section 3 we introduce the classical Dirichlet–Neumann and the new Robin–Robin partitioned procedures. Sections 3.1 and 3.2 are devoted to the two simplified models used to provide suitable coefficients for the Robin boundary conditions. In Section 4 we introduce the algebraic counterpart of the FSI problem and we interpret the partitioned procedures as a block Gauss–Seidel iterative solver. The convergence analysis of the DN, RN and RD schemes is carried out in Section 5. A meaningful set of numerical experiments are presented in Section 6, that confirm all the theoretical results obtained in Section 5. Finally, in Section 7 we draw some conclusions.

2. Problem setting

Let us consider an heterogeneous mechanical system which covers a bounded and moving domain $\Omega^t \subset \mathbb{R}^d$ ($d = 2, 3$, being the space dimension), where t here denotes time. This domain is divided into a sub-domain Ω_s^t occupied by an elastic structure and its complement Ω_f^t occupied by the fluid. The fluid–structure interface Σ^t is the common boundary between Ω_s^t and Ω_f^t, i.e. $\Sigma^t = \partial\Omega_f^t \cap \partial\Omega_s^t$. Furthermore, $\boldsymbol{n}_f$ is the outward normal to Ω_f^t on Σ^t and $\boldsymbol{n}_s = -\boldsymbol{n}_f$ is its counterpart for the structure domain. The initial configuration Ω^0 at $t = 0$ is considered as the reference one.

In order to describe the evolution of the whole domain Ω^t we define two families of mappings:

$$\mathcal{L} : \Omega_s^0 \times (0, T) \rightarrow \Omega_s^t, \quad (\boldsymbol{x}_0, t) \mapsto \boldsymbol{x} = \mathcal{L}(\boldsymbol{x}_0, t)$$

and

$$\mathcal{A} : \Omega_f^0 \times (0, T) \rightarrow \Omega_f^t, \quad (\boldsymbol{x}_0, t) \mapsto \boldsymbol{x} = \mathcal{A}(\boldsymbol{x}_0, t).$$

The map $\mathcal{L}^t = \mathcal{L}(\cdot, t)$ tracks the solid domain in time and $\mathcal{A}^t = \mathcal{A}(\cdot, t)$ does the same with the fluid domain. The combination of these two mappings define an homeomorphism over Ω^t under the following continuity condition on the interface:

$$\mathcal{L}^t = \mathcal{A}^t \quad \text{on } \Sigma^t \; \forall t \in (0, T). \tag{1}$$

We adopt a purely Lagrangian approach to describe the structure kinematics. Therefore, the solid mapping is straightforwardly determined by

$$\mathcal{L}^t(\boldsymbol{x}_0) = \boldsymbol{x}_0 + \hat{\boldsymbol{\eta}}(\boldsymbol{x}_0, t),$$

where $\hat{\boldsymbol{\eta}}$ denotes the displacement of the solid medium with respect to the reference configuration.

The fluid problem is stated in an Arbitrary Lagrangian–Eulerian (ALE) framework (see e.g. [12,6]). The fluid domain mapping $\mathcal{A}^t$ is defined by an appropriate extension of its value on the interface, which is given by condition (1):

$$\mathcal{A}^t(\boldsymbol{x}_0) = \boldsymbol{x}_0 + \text{Ext}(\hat{\boldsymbol{\eta}}(\boldsymbol{x}_0, t)|_{\Sigma^0}). \tag{2}$$

A classical choice is to consider a harmonic extension operator in the reference domain. In general, this mapping does not track the fluid particles.

For any function $\hat{g} : \Omega_s^0 \times (0, T) \to \mathbb{R}$ defined in the reference solid configuration, we denote by $g = \hat{g} \circ (\mathcal{L}^t)^{-1}$ its counterpart in the current domain:

$$g : \Omega_s^t \times (0, T) \to \mathbb{R}, \quad g(\boldsymbol{x}, t) = \hat{g}((\mathcal{L}^t)^{-1}(\boldsymbol{x}), t).$$

An analogous notation is adopted for the fluid domain: given $f : \Omega_f^t \times (0, T) \to \mathbb{R}$ defined in the current fluid configuration, we denote by $\hat{f} = f \circ \mathcal{A}^t$ its counterpart in the reference fluid domain:

$$\hat{f} : \Omega_f^0 \times (0, T) \to \mathbb{R}, \quad \hat{f}(\boldsymbol{x}_0, t) = f(\mathcal{A}^t(\boldsymbol{x}_0), t).$$

We define the ALE time derivative as follows:

$$\partial_t f|_{\boldsymbol{x}_0} : \Omega_f^t \times (0, T) \to \mathbb{R}, \quad \partial_t f|_{\boldsymbol{x}_0}(\boldsymbol{x}, t) = \partial_t \hat{f} \circ (\mathcal{A}^t)^{-1}(\boldsymbol{x}).$$

Moreover, we calculate the fluid domain velocity $\boldsymbol{w}$ as

$$\boldsymbol{w}(\boldsymbol{x}, t) = \partial_t \boldsymbol{x}|_{\boldsymbol{x}_0} = \partial_t \mathcal{A}^t \circ (\mathcal{A}^t)^{-1}(\boldsymbol{x}).$$

Then, owing to (2), we have

$$\hat{\boldsymbol{w}}(\boldsymbol{x}_0, t) = \text{Ext}(\partial_t \hat{\boldsymbol{\eta}}(\boldsymbol{x}_0, t)|_{\Sigma^0})$$

provided that the extension operator chosen interchanges with the time derivatives.

The solid is assumed to be an elastic material, characterized by a constitutive law relating the Cauchy stress tensor $\boldsymbol{T}_s$ to the deformation gradient $\boldsymbol{F}(\hat{\boldsymbol{\eta}}) = \boldsymbol{I} + \nabla \hat{\boldsymbol{\eta}}$. Moreover, we assume the fluid to be homogeneous, Newtonian and incompressible. We indicate with $\boldsymbol{T}_f$ its Cauchy stress tensor:

$$\boldsymbol{T}_f(\boldsymbol{u}, p) = -p\boldsymbol{I} + 2\mu \boldsymbol{G}(\boldsymbol{u}),$$

where p is the pressure, μ the dynamic viscosity and

$$\boldsymbol{G}(\boldsymbol{u}) = \frac{1}{2}(\nabla \boldsymbol{u} + (\nabla \boldsymbol{u})^{\mathrm{T}})$$

is the strain rate tensor.

In order to write the fluid problem in ALE form, let us apply the chain rule to the velocity time derivative:

$$\partial_t \boldsymbol{u}|_{\boldsymbol{x}_0} = \partial_t \boldsymbol{u} + \boldsymbol{w} \cdot \nabla \boldsymbol{u},$$

where $\partial_t \boldsymbol{u}$ is the partial time derivative in the spatial frame (Eulerian derivative).

Then, the fluid–structure problem in strong form reads:

1. Fluid–structure problem. Find the fluid velocity $\boldsymbol{u}$, pressure p and the structure displacement $\hat{\boldsymbol{\eta}}$ such that

$$\rho_f \partial_t \boldsymbol{u}|_{\boldsymbol{x}_0} + \rho_f (\boldsymbol{u} - \boldsymbol{w}) \cdot \nabla \boldsymbol{u} - \nabla \cdot \boldsymbol{T}_f = \boldsymbol{f}_f \quad \text{in } \Omega_f^t \times (0, T), \tag{3a}$$

$$\nabla \cdot \boldsymbol{u} = 0 \quad \text{in } \Omega_f^t \times (0, T), \tag{3b}$$

$$\rho_s \partial_{tt} \hat{\boldsymbol{\eta}} - \nabla \cdot \hat{\boldsymbol{T}}_s = \hat{\boldsymbol{f}}_s \quad \text{in } \Omega_s^0 \times (0, T), \tag{3c}$$

$$\boldsymbol{u} = \partial_t \boldsymbol{\eta} \quad \text{on } \Sigma^t \times (0, T), \tag{3d}$$

$$\boldsymbol{T}_s \cdot \boldsymbol{n}_s + \boldsymbol{T}_f \cdot \boldsymbol{n}_f = 0 \quad \text{on } \Sigma^t \times (0, T). \tag{3e}$$

2. Geometry problem. Find the fluid domain displacement

$$\mathcal{A}^t(\boldsymbol{x}_0) = \boldsymbol{x}_0 + \text{Ext}(\hat{\boldsymbol{\eta}}|_{\Sigma^0}), \quad \boldsymbol{w} = \partial_t \mathcal{A}^t \circ (\mathcal{A}^t)^{-1}, \quad \Omega_f^t = \mathcal{A}^t(\Omega_f^0). \tag{4}$$

Here, ρ_f and ρ_s are the fluid and structure densities and $\boldsymbol{f}_f$ and $\hat{\boldsymbol{f}}_s$ the forcing terms. Two transmission conditions are enforced at the interface: the continuity of fluid and structure velocities (3d), due to the adherence condition, and the *continuity of stresses* (3e), expressing the action–reaction principle. The fluid and structure problems are also coupled by the *geometrical condition* (4), leading to a highly nonlinear problem. Finally, system (3) and (4) has to be endowed with suitable boundary conditions on $\partial \Omega^t \setminus \Sigma^t$ and initial conditions. Since the choice of boundary and initial conditions is not essential in the forecoming discussion, they will not be detailed here.

2.1. The time discrete system

In this section we discretize in time system (3) and (4). Let Δt be the time step size and $t^n = n \Delta t$ for $n = 0, \dots, N$. We denote by z^n the approximation of a time dependent function z at time level t^n. Let us define the backward difference operator δ_t as $\delta_t z^{n+1} = (z^{n+1} - z^n)/\Delta t$. The discrete ALE derivative is evaluated by the following expression:

$$\delta_t z^{n+1}|_{\boldsymbol{x}_0} = (z^{n+1} - z^n \circ \mathcal{A}^n \circ (\mathcal{A}^{n+1})^{-1})/\Delta t.$$

We consider a backward Euler scheme for the time discretization of the fluid problem and an implicit first order BDF scheme for the structure problem. Observe, however, that all the partitioned procedures proposed in this work can be easily extended to other time marching schemes.

In order to treat the nonlinearity given by the convective term and by the fluid domain, we detail two strategies; the semi-implicit and the implicit algorithms (see e.g. [1,16]). In the first case, we use suitable extrapolations $\Omega_f^*, \boldsymbol{u}^*$ and $\boldsymbol{w}^*$ of the fluid domain, fluid velocity and fluid domain velocity, respectively, obtaining the following algorithm:

2.2. Semi-implicit algorithm

Given $\boldsymbol{u}^n, \hat{\boldsymbol{\eta}}^n, \hat{\boldsymbol{\eta}}^{n-1}$ and Ω_f^n, for each n

1. Build a suitable extrapolation Ω_f^* of the domain Ω_f^{n+1}.
2. Solve the linearized FSI problem

$$\rho_f \delta_t \boldsymbol{u}^{n+1} + \rho_f (\boldsymbol{u}^* - \boldsymbol{w}^*) \cdot \nabla \boldsymbol{u}^{n+1} - \nabla \cdot \boldsymbol{T}_f^{n+1} = \boldsymbol{f}_f^{n+1} \quad \text{in } \Omega_f^*, \tag{5a}$$

$$\nabla \cdot \boldsymbol{u}^{n+1} = 0 \quad \text{in } \Omega_f^*, \tag{5b}$$

$$\rho_s \delta_{tt} \hat{\boldsymbol{\eta}}^{n+1} - \nabla \cdot \hat{\boldsymbol{T}}_s^{n+1} = \hat{\boldsymbol{f}}_s^{n+1} \quad \text{in } \Omega_0^s, \tag{5c}$$

$$\boldsymbol{u}^{n+1} = \delta_t \boldsymbol{\eta}^{n+1} \quad \text{on } \Sigma^*, \tag{5d}$$

$$\boldsymbol{T}_s^{n+1} \cdot \boldsymbol{n}_s + \boldsymbol{T}_f^{n+1} \cdot \boldsymbol{n}_f = 0 \quad \text{on } \Sigma^*, \tag{5e}$$

3. Update the fluid domain

$$\mathcal{A}^{n+1}(\boldsymbol{x}^0) = \boldsymbol{x}^0 + \text{Ext}(\hat{\boldsymbol{\eta}}^{n+1}|_{\Sigma^0}),$$

$$\boldsymbol{w}^{n+1} = \delta_t \mathcal{A}^{n+1} \circ (\mathcal{A}^{n+1})^{-1}, \quad \Omega_f^{n+1} = \mathcal{A}^{n+1}(\Omega_f^0),$$

where we have set $\delta_{tt}(\cdot) = \delta_t(\delta_t(\cdot))$. A simple choice is given by the first order extrapolations $\Omega_f^* = \Omega_f^n, \boldsymbol{u}^* = \boldsymbol{u}^n$ and $\boldsymbol{w}^* = \boldsymbol{w}^n$.

A second possibility is to treat implicitly the fluid domain and the convective term and to embed the previous fluid–structure scheme into a fixed-point loop on the position of the FS interface Σ^*. Indicating with i the sub-iterations index, we obtain the following:

2.3. Implicit algorithm

Given $\boldsymbol{u}^n, \hat{\boldsymbol{\eta}}^n, \hat{\boldsymbol{\eta}}^{n-1}$ and Ω_f^n, for $i = 0, 1, \ldots$ do until convergence.

1. Solve the linearized FSI problem

$$\rho_f \delta_t \boldsymbol{u}_{i+1}^{n+1} + \rho_f (\boldsymbol{u}_i^{n+1} - \boldsymbol{w}_i^{n+1}) \cdot \nabla \boldsymbol{u}_{i+1}^{n+1} - \nabla \cdot \boldsymbol{T}_{f,i+1}^{n+1} = \boldsymbol{f}_f^{n+1} \quad \text{in } \Omega_{f,i}^{n+1}, \tag{6a}$$

$$\nabla \cdot \boldsymbol{u}_{i+1}^{n+1} = 0 \quad \text{in } \Omega_{f,i}^{n+1}, \tag{6b}$$

$$\rho_s \delta_{tt} \hat{\boldsymbol{\eta}}_{i+1}^{n+1} - \nabla \cdot \hat{\boldsymbol{T}}_{s,i+1}^{n+1} = \hat{\boldsymbol{f}}_s^{n+1} \quad \text{in } \Omega_0^s, \tag{6c}$$

$$\boldsymbol{u}_{i+1}^{n+1} = \delta_t \boldsymbol{\eta}_{i+1}^{n+1} \quad \text{on } \Sigma_i^{n+1}, \tag{6d}$$

$$\boldsymbol{T}_{s,i+1}^{n+1} \cdot \boldsymbol{n}_s + \boldsymbol{T}_{f,i+1}^{n+1} \cdot \boldsymbol{n}_f = 0 \quad \text{on } \Sigma_i^{n+1}. \tag{6e}$$

2. Update the fluid domain

$$\mathcal{A}_{i+1}^{n+1}(\boldsymbol{x}^0) = \boldsymbol{x}^0 + \text{Ext}(\hat{\boldsymbol{\eta}}_{i+1}^{n+1}|_{\Sigma^0}),$$

$$\boldsymbol{w}_{i+1}^{n+1} = \delta_t \mathcal{A}_{i+1}^{n+1} \circ (\mathcal{A}_{i+1}^{n+1})^{-1}, \quad \Omega_{f,i+1}^{n+1} = \mathcal{A}_{i+1}^{n+1}(\Omega_f^0).$$

System (5) (as well as every fixed-point iteration of (6)) is a fully coupled and linearized fluid–structure problem, where the transmission conditions (5d) and (5e) are kept implicit. In case of using a nonlinear structural model, the linearization of the structure sub-problem should also be considered.

Our goal is then to devise partitioned procedures for the solution of such a linearized problem. Partitioned strategies capable of splitting the linear FSI problem into two separate sub-problems are very appealing from a computational point of view, since they allow one to reuse codes that have been developed for each field separately. This is the motivation of the *partitioned procedures* introduced in the next section.

3. Robin–Robin partitioned procedures

Partitioned procedures have been introduced in order to solve the linearized fluid–structure system by separate evaluations of fluid and structure sub-problems. These iterative algorithms can be motivated from a domain decomposition viewpoint (see e.g. [5]). The most widely used partitioned procedure is the Dirichlet–Neumann (DN) technique, that consists in solving the fluid sub-problem with a Dirichlet boundary condition and the structure sub-problem with a Neumann boundary condition. We recall it briefly here. To lighten the notation we omit here and in what follows the temporal index n. Referring to the semi-implicit scheme, system (5), and indicating with k the sub-iteration index, the DN algorithm reads:

Dirichlet–Neumann algorithm
Given $\boldsymbol{\eta}^n, \boldsymbol{\eta}^{n-1}, \boldsymbol{u}^n$ and the current iteration $\boldsymbol{\eta}^k$, find the next iteration $\boldsymbol{\eta}^{k+1}, \boldsymbol{u}^{k+1}$ and p^{k+1} such that,

1. Fluid problem (Dirichlet boundary condition)

$$\rho_f \delta_t \boldsymbol{u}^{k+1} + \rho_f (\boldsymbol{u}^* - \boldsymbol{w}^*) \cdot \nabla \boldsymbol{u}^{k+1} - \nabla \cdot \boldsymbol{T}_f^{k+1} = \boldsymbol{f}_f \quad \text{in } \Omega_f^*,$$

$$\nabla \cdot \boldsymbol{u}^{k+1} = 0 \quad \text{in } \Omega_f^*,$$

$$\boldsymbol{u}^{k+1} = \delta_t \boldsymbol{\eta}^k \quad \text{on } \Sigma^*.$$

2. Structure problem (Neumann boundary condition)

$$\rho_s \delta_{tt} \hat{\boldsymbol{\eta}}^{k+1} - \nabla \hat{\boldsymbol{T}}_s^{k+1} = \hat{\boldsymbol{f}}_s \quad \text{in } \Omega_0^s,$$

$$\boldsymbol{T}_s^{k+1} \cdot \boldsymbol{n}_s = -\boldsymbol{T}_f^{k+1} \cdot \boldsymbol{n}_f \quad \text{on } \Sigma^*.$$

Once convergence is achieved, the geometry problem is solved and the new domain updated. Obviously, the order in which the two sub-problems are solved can be reversed.

Remark 1. The same strategy can be applied in the implicit case to solve the linearized FSI problem (6). This leads to a two nested loops algorithm. We point out that the internal loop does not need to be solved to full accuracy and in general it is enough to reduce the initial residual by a given factor.

Alternatively, one could decide to perform only one iteration in the internal loop, which would lead to the "classical" non-linear DN (fixed-point) algorithm, considered for example in [15,20,5].

Unfortunately, the convergence properties of this algorithm deteriorate for certain classes of problems, like the blood-vessel system. This phenomenon is related to the added-mass effect. Roughly speaking, this effect becomes critical when fluid and structure densities are of the same order or when the domain is very slender. We refer to [3] for a discussion on the added-mass effect in the frame of partitioned procedures. The straight-forward alternative to DN is the Neumann–Dirichlet (ND) partitioned procedure. However, this scheme has even worse numerical properties. In [5] a Neumann–Neumann algorithm was also proposed for hemodynam-ics problems. Yet the results obtained did not improve substantially those obtained with a simple DN algorithm. As a conclusion, the existing partitioned procedures are not suitable for some interesting FSI prob-lems, as those encountered in hemodynamics applications.

At this point, let us consider a linear combination of the continuity of velocities and stresses conditions that leads to a new set of transmission conditions of Robin type. These new transmission conditions lead to a new family of partitioned procedures, introduced with the aim of getting better convergence properties.

In particular, referring to the semi-implicit case, we replace (5d) and (5e) by the following set of (equivalent) transmission conditions

$$
\begin{aligned}
\alpha_f \boldsymbol{u}^{n+1} + \boldsymbol{T}_f^{n+1} \cdot \boldsymbol{n}_f &= \alpha_f \delta_t \boldsymbol{\eta}^{n+1} - \boldsymbol{T}_s^{n+1} \cdot \boldsymbol{n}_s \quad \text{on } \Sigma^*, \\
\frac{\alpha_s}{\Delta t} \boldsymbol{\eta}^{n+1} + \boldsymbol{T}_s^{n+1} \cdot \boldsymbol{n}_s &= \frac{\alpha_s}{\Delta t} \boldsymbol{\eta}^n + \alpha_s \boldsymbol{u}^{n+1} - \boldsymbol{T}_f^{n+1} \cdot \boldsymbol{n}_f \quad \text{on } \Sigma^*,
\end{aligned}
\tag{7}
$$

where the combination parameters must satisfy $\alpha_f \neq -\alpha_s$. Moreover, to have well-posed sub-problems we will assume $\alpha_f, \alpha_s > 0$. By doing this, we are replacing Dirichlet and Neumann boundary conditions by two Robin boundary conditions on the FSI interface. Let us introduce now the Robin–Robin (RR) algorithm for the solution of system (5), omitting for the sake of simplicity the time index $n + 1$:

Robin–Robin algorithm

Given $\boldsymbol{\eta}^n, \boldsymbol{\eta}^{n-1}, \boldsymbol{u}^n$ and the current iteration $\boldsymbol{\eta}^k$, find the next iteration $\boldsymbol{\eta}^{k+1}, \boldsymbol{u}^{k+1}$ and p^{k+1} such that,

1. Fluid problem (Robin boundary condition)

$$
\rho_f \delta_t \boldsymbol{u}^{k+1} + \rho_f (\boldsymbol{u}^* - \boldsymbol{w}^*) \cdot \nabla \boldsymbol{u}^{k+1} - \nabla \cdot \boldsymbol{T}_f^{k+1} = \boldsymbol{f}_f \quad \text{in } \Omega_f^*,
\tag{8a}
$$

$$
\nabla \cdot \boldsymbol{u}^{k+1} = 0 \quad \text{in } \Omega_f^*,
\tag{8b}
$$

$$
\alpha_f \boldsymbol{u}^{k+1} + \boldsymbol{T}_f^{k+1} \cdot \boldsymbol{n}_f = \alpha_f \delta_t \boldsymbol{\eta}^k - \boldsymbol{T}_s^k \cdot \boldsymbol{n}_s \quad \text{on } \Sigma^*.
\tag{8c}
$$

2. Structure problem (Robin boundary condition)

$$
\rho_s \delta_{tt} \hat{\boldsymbol{\eta}}^{k+1} - \nabla \cdot \hat{\boldsymbol{T}}_s^{k+1} = \hat{\boldsymbol{f}}_s \quad \text{in } \Omega_0^s,
\tag{9a}
$$

$$
\frac{\alpha_s}{\Delta t} \boldsymbol{\eta}^{k+1} + \boldsymbol{T}_s^{k+1} \cdot \boldsymbol{n}_s = \frac{\alpha_s}{\Delta t} \boldsymbol{\eta}^n + \alpha_s \boldsymbol{u}^{k+1} - \boldsymbol{T}_f^{k+1} \cdot \boldsymbol{n}_f \quad \text{on } \Sigma^*.
\tag{9b}
$$

The RR partitioned procedure can be applied to the implicit system (6) as well, as described in Remark 1.

The Robin–Robin algorithm generates a family of partitioned procedures. Indeed, the classical DN and ND algorithms can be recovered with appropriate values of the combination parameters. We can also consider the particular cases $\alpha_f = 0$ or $\alpha_s = 0$, leading to the Neumann–Robin and the Robin–Neumann schemes, respectively. Dirichlet–Robin and Robin–Dirichlet schemes are obtained taking (conceptually) $\alpha_f = \infty$ and $\alpha_s = \infty$, respectively. We summarize all these methods in Table 1, where p.b.v. stands for "positive and bounded value".

Table 1
Family of partitioned procedure generated by Robin transmission conditions

Algorithm	α_f	α_s
Dirichlet–Neumann	∞	0
Neumann–Dirichlet	0	∞
Robin–Dirichlet	p.b.v.	∞
Dirichlet–Robin	∞	p.b.v.
Robin–Neumann	p.b.v.	0
Neumann–Robin	0	p.b.v.
Robin–Robin	p.b.v.	p.b.v.

At this point, the main issue is the evaluation of suitable combination parameters α_f and α_s that will improve the convergence properties of the classical DN scheme. In the next section we provide a way to estimate such parameters, based on two simplified models for the fluid and for the structure problems.

3.1. Simplified structure model

We consider the membrane model proposed in [16] as a simplified model for the structure. We point out that this is a lower dimensional model describing the structure as a $(d-1)$-dimensional manifold coinciding with Σ^0. Following [16], the reference position Σ^0 of the membrane is identified by a regular mapping

$$\boldsymbol{\phi} : \omega \subset \mathbb{R}^2 \to \Sigma^0 \subset \mathbb{R}^3, \quad \boldsymbol{\phi} = \boldsymbol{\phi}(\xi_1, \xi_2) \ \forall (\xi_1, \xi_2) \in \omega.$$

Under the hypothesis of small deformations, negligible bending terms and only normal displacement, the structure model reduces to the simple scalar equation (inertial-algebraic model)

$$\rho_s H_s \frac{\partial^2 \eta}{\partial t^2} + \beta \eta = f_s - \boldsymbol{n}_f \cdot (\boldsymbol{T}_f \cdot \boldsymbol{n}_f) \quad \text{in } \Sigma^t \times (0, T), \tag{10}$$

where η and f_s are the normal components of the structure displacement and body force (in the direction $\boldsymbol{n}_f$), respectively, and β is the *algebraic parameter*

$$\beta = \beta(\xi_1, \xi_2) = \frac{H_s E}{1 - v^2} (4\rho_1^2 - 2(1 - v)\rho_2),$$

where E and v are the Young modulus and the Poisson coefficient of the material at hand, H_s is the thickness of the structure and ρ_1 and ρ_2 are the mean and Gaussian curvature of Σ^0. Then, setting $u = \boldsymbol{u} \cdot \boldsymbol{n}_f$ and $T_f = \boldsymbol{n}_f \cdot (\boldsymbol{T}_f \cdot \boldsymbol{n}_f)$ and owing to (5d) (or (6d)), the fluid–structure interaction problem (5) (or (6)) is reduced to a fluid problem supplemented with a Robin transmission condition at the interface for the normal component of the velocity, namely

$$\left(\frac{\rho_s H_s}{\Delta t} + \beta \Delta t \right) u^{n+1} + T_f^{n+1} = f_s^{n+1} + \left(\frac{\rho_s H_s}{\Delta t^2} - \beta \right) \eta^n - \frac{\rho_s H_s}{\Delta t^2} \eta^{n-1} \quad \text{on } \Sigma^*. \tag{11}$$

In the case of a membrane structure and for an inertial-algebraic law the fulfillment of the interface conditions (5d) and (5e) is guaranteed in just one iteration between the fluid and structure problems (in fact, the structure problem is not explicitly solved since it is embedded in the fluid one thanks to (11)). In the case of a d dimensional structure and for more general structure models, whose behaviour, however, is similar to the one predicted by (10), the previous derivation suggests the use of Robin transmission condition as in (8c) with coefficient

$$\alpha_f = \frac{\rho_s H_s}{\Delta t} + \beta \Delta t \tag{12}$$

inferred from (11). We observe that this value is easily computed, since it depends on the physical and geometrical properties of the structure at hand and on the time step. As an example, when the geometry of the structure is a cylinder, $\beta = H_s E / ((1 - v^2) R^2)$, where R is the radius of the cylinder.

We point out that (11) prescribes a boundary condition at the interface in the normal direction only. However, for easiness of implementation we propose to use a Robin boundary condition with the same coefficient α_f also in tangential directions as written in (8c).

3.2. Simplified fluid model

The motivation of this section is to derive a simplified fluid model that would allow us to quantify the added mass effect on the structure. Our goal is to find an algebraic operator relating the fluid normal stress at the interface to the structure acceleration. Unfortunately, the operator describing the added mass effect is not algebraic and its approximation by an algebraic relationship is not evident.

We consider the simplified fluid model proposed in [3]. In particular, the fluid is described by a linear incompressible inviscid model, imposing at the interface the structure velocity. We also assume small displacements for the structure, which implies that the fluid domain can be kept fixed. We denote by $\eta = \boldsymbol{\eta} \cdot n_f$ the displacement of the structure in the direction $\boldsymbol{n}_f$ and again $u = \boldsymbol{u} \cdot \boldsymbol{n}_f$. Let us consider the following simplified model:

$$
\begin{aligned}
&\rho_f \partial_t \boldsymbol{u} + \nabla p = \boldsymbol{0} \quad \text{in } \Omega_f \times (0, T), \\
&\nabla \cdot \boldsymbol{u} = 0 \quad \text{in } \Omega_f \times (0, T), \\
&u = \partial_t \eta \quad \text{on } \Sigma \times (0, T)
\end{aligned} \tag{13}
$$

with suitable boundary conditions on $\partial \Omega_f \setminus \Sigma$ and initial conditions. The time discretization of (13) using backward Euler at time step $n + 1$ reads

$$
\rho_f \delta_t \boldsymbol{u}^{n+1} + \nabla p^{n+1} = \boldsymbol{0} \quad \text{in } \Omega_f, \tag{14a}
$$

$$
\nabla \cdot \boldsymbol{u}^{n+1} = 0 \quad \text{in } \Omega_f, \tag{14b}
$$

$$
u^{n+1} = \delta_t \boldsymbol{\eta}^{n+1} \quad \text{on } \Sigma. \tag{14c}
$$

In this system, the value of the pressure on the interface can be written as a function of the imposed interface acceleration

$$
p^{n+1} = -\rho_f \mathcal{M}(\delta_t u^{n+1}) + \hat{p}^{n+1} \quad \text{on } \Sigma,
$$

where $\hat{p}^{n+1}$ takes into account non-homogeneous boundary conditions on $\partial \Omega_f \setminus \Sigma$ and $\mathcal{M} : H^{-1/2}(\Sigma) \to H^{1/2}(\Sigma)$ stands for the *added-mass* operator. Observe that this operator, relating the interface pressure and acceleration is not algebraic. We refer to Section 5 for a detailed description of this operator. For this simplified problem, the stress exerted by the fluid on the structure in the normal direction is simply p^{n+1} and the continuity of normal stresses at the interface becomes

$$
T_s^{n+1} = T_f^{n+1} = \rho_f \mathcal{M}(\delta_t u^{n+1}) - \hat{p}^{n+1} = \rho_f \mathcal{M}(\delta_{tt} \eta^{n+1}) - \hat{p}^{n+1},
$$

where we have set $T_f = \boldsymbol{n}_f \cdot (\boldsymbol{T}_f \cdot \boldsymbol{n}_f)$ and $T_s = \boldsymbol{n}_s \cdot (\boldsymbol{T}_s \cdot \boldsymbol{n}_s)$. From the previous relationship we obtain the following generalized Robin boundary condition for the structure in the normal direction

$$
\frac{\rho_f \mathcal{M}}{\Delta t^2} \boldsymbol{\eta}^{n+1} \cdot \boldsymbol{n}_s + \boldsymbol{n}_s \cdot (\boldsymbol{T}_s^{n+1} \cdot \boldsymbol{n}_s) = \frac{\rho_f \mathcal{M}}{\Delta t^2} (2 \boldsymbol{\eta}^n - \boldsymbol{\eta}^{n-1}) \cdot \boldsymbol{n}_s - \hat{p}^{n+1} \boldsymbol{n}_s. \tag{15}
$$

Condition (15) embeds the fluid problem into the structure problem. Thus, the interface condition is again satisfied in just one iteration. The generalized Robin condition (15) can be obtained from (9b) by taking $\alpha_s = (\rho_f / \Delta t^2) \mathcal{M}(\cdot)$. In order to obtain a "classical" Robin condition, we propose to approximate the operator $\mathcal{M}$ by $\gamma \mu_{\max} I$, where $\mu_{\max}$ is the maximum eigenvalue of the added-mass operator, I is the identity operator and γ is a coefficient suitably chosen, getting

$$
\alpha_s = \gamma \frac{\rho_f \mu_{\max}}{\Delta t}. \tag{16}
$$

In the case of a fluid governed by the Navier–Stokes equations, the embedding of the fluid problem into the structure one is not an easy task. However, we propose to use again partitioned procedures with Robin bound-

ary conditions as in (9b) with the coefficient (16) based on the approximation of the added-mass operator using its largest eigenvalue.

Although the choice (16) is only heuristic, the numerical tests presented in Section 6 reveal that this is a very reasonable choice. The scaling factor γ has to be tuned to obtain good convergence properties. Yet, the tuned value seems to be very robust and practically independent of ρ_f, Δt and some geometrical parameters defining the physical domain (and then μ_{max}). This indicates that formula (16) captures the correct dependence of the coefficient α_s on the physical parameters of the problems.

We point out that the analytical evaluation of μ_{max} is not straightforward for a general geometry and we have to resort to a numerical approximation. However, as we will show in Section 5, it is possible to provide an analytical expression of μ_{max} for particular geometries.

Finally, as for the simplified structure model, we propose to apply the Robin transmission condition on the structure, with parameter α_s given by (16), on both the normal and tangential directions, for easiness of implementation.

4. Block Gauss–Seidel interpretation

In this section we motivate the partitioned procedures introduced above from an algebraic point of view. We have only considered the semi-implicit case for the sake of simplicity, but the extension to the implicit case is straightforward. The fully coupled algebraic FSI system is obtained by writing the weak form of the semi-discrete FSI problem (5) and discretizing it in space using the finite element method. In particular, let us introduce a triangulation of the fluid and structure domains and assume that the two meshes are conforming on the fluid–structure interface Σ^t. Moreover, we consider suitable finite element spaces with Lagrangian basis functions, so that the degrees of freedom correspond to nodal values of the solution. We skip the details and refer to [1] for a detailed discussion. We end up with the following linear system:

$$A\mathbf{X}^{n+1} = \mathbf{b}^{n+1}, \tag{17}$$

where

$$A = \begin{bmatrix} C_{ff} & G_f & C_{f\Sigma} & 0 & 0 \\ D_f & 0 & D_s & 0 & 0 \\ 0 & 0 & M_\Sigma & -M_\Sigma/\Delta t & 0 \\ C_{\Sigma f} & G_\Sigma & C_{\Sigma\Sigma} & S_{\Sigma\Sigma} & S_{\Sigma s} \\ 0 & 0 & 0 & S_{s\Sigma} & S_{ss} \end{bmatrix}, \tag{18}$$

$$\mathbf{X}^{n+1} = \begin{bmatrix} \mathbf{U}_f^{n+1} \\ \mathbf{P}^{n+1} \\ \mathbf{U}_\Sigma^{n+1} \\ \mathbf{D}_\Sigma^{n+1} \\ \mathbf{D}_s^{n+1} \end{bmatrix}, \quad \mathbf{b}^{n+1} = \begin{bmatrix} \mathbf{b}_f^{n+1} \\ \mathbf{0} \\ -M_\Sigma/\Delta t \mathbf{D}_\Sigma^n \\ \mathbf{b}_\Sigma^{n+1} \\ \mathbf{b}_s^{n+1} \end{bmatrix}. \tag{19}$$

Here, $\mathbf{U}_f^{n+1}$ is the vector of nodal values of the fluid velocity on the interior nodes, $\mathbf{U}_\Sigma^{n+1}$ are the fluid velocity nodal values on the interface, $\mathbf{P}^{n+1}$ is the vector of (interior and interface) nodal values for the pressure. Finally, $\mathbf{D}_s^{n+1}$ and $\mathbf{D}_\Sigma^{n+1}$ are the vectors of structure displacements related to interior and interface nodes, respectively. On the other hand, the right hand side $\mathbf{b}^{n+1}$ accounts for external forces and other terms related to the time discretization scheme. The first two rows are the fully discrete versions of the momentum and mass conservation equations for the fluid. The third equation states the continuity of velocities on the interface and is the algebraic counterpart of (5d). We have indicated by M_Σ the interface mass matrix, which is invertible. The fourth row enforces continuity of stresses in a weak form. Finally, the fifth row is the structure problem in the internal nodes. If non-conforming meshes are considered, the third and fourth row should be modified accordingly by introducing a projection (or interpolation) matrix between the interface structure displacement and fluid velocity finite element spaces (see, e.g. [15]).

All the partitioned procedures introduced so far can be written as a block Gauss–Seidel (GS) iterative solver for the preconditioned system

$$P^{-1}A\mathbf{X}^{n+1} = P^{-1}\mathbf{b}^{n+1},$$

where P is a suitable *preconditioning matrix* which will be detailed later. We consider the following partition of the unknowns vector $\mathbf{X}^{n+1}$ into

$$\mathbf{X}_f^{n+1} = \begin{bmatrix} \mathbf{U}_f^{n+1} \\ \mathbf{P}^{n+1} \\ \mathbf{U}_\Sigma^{n+1} \end{bmatrix}, \quad \mathbf{X}_s^{n+1} = \begin{bmatrix} \mathbf{D}_\Sigma^{n+1} \\ \mathbf{D}_s^{n+1} \end{bmatrix}.$$

This choice splits the FSI system into "fluid" and "structure" blocks. This is the only choice that allows modularity of FSI codes. Let us denote the blocks of PA and $P\mathbf{b}^{n+1}$ as

$$PA =: \begin{bmatrix} B_{ff} & B_{fs} \\ B_{sf} & B_{ss} \end{bmatrix}, \quad P\mathbf{b}^{n+1} =: \begin{bmatrix} (P\mathbf{b}^{n+1})_f \\ (P\mathbf{b}^{n+1})_s \end{bmatrix}.$$

Therefore, omitting for the sake of simplicity the time index $n + 1$, an abstract block Gauss–Seidel procedure for the solution of the fluid–structure system (17) at time step $n + 1$ consists of given $\mathbf{X}^k$, do until convergence

$$B_{ff}\mathbf{X}_f^{k+1} = (P\mathbf{b})_f - B_{fs}\mathbf{X}_f^k,$$
$$B_{ss}\mathbf{X}_s^{k+1} = (P\mathbf{b})_s - B_{sf}\mathbf{X}_f^{k+1}.$$

We supplement this iterative procedure with the following stopping criterion:

$$\frac{\|\mathbf{r}^{k+1}\|}{\|\mathbf{r}^0\|} := \frac{\|\mathbf{b} - A\mathbf{X}^{k+1}\|}{\|\mathbf{b} - A\mathbf{X}^0\|} < \varepsilon \tag{20}$$

for a suitable tolerance ε. Criterion (20) requires to evaluate the residual of the FSI monolithic system (17).

In this frame we can recover the DN, ND and RR partitioned procedures, by designing the respective preconditioning matrices. For instance, for the DN algorithm, the preconditioning matrix is the identity matrix. In this case, it is easy to show that the residual reduces to

$$\mathbf{r}_D^{k+1} := -M_\Sigma\mathbf{U}_\Sigma^{k+1} + M_\Sigma\delta_t\mathbf{D}_\Sigma^{k+1}, \tag{21}$$

that is, we have to check that the continuity of the velocity at the interface is satisfied up to a given tolerance. We point out that, since we start with a Dirichlet problem, the continuity of the stresses is exactly satisfied at each sub-iteration. On the contrary, if we consider the re-ordered system in which the structure is solved first, the stopping criterion changes and the residual becomes

$$\mathbf{r}_N^{k+1} := \mathbf{b}_\Sigma - C_{\Sigma f}\mathbf{U}_f^{k+1} - G_\Sigma\mathbf{P}^{k+1} - C_{\Sigma\Sigma}\mathbf{U}_\Sigma^{k+1} - S_{\Sigma\Sigma}\mathbf{D}_\Sigma^{k+1} - S_{\Sigma s}\mathbf{D}_s^{k+1}. \tag{22}$$

The new Robin-type partitioned procedures introduced in this article can be obtained using a preconditioning matrix

$$P_{RR} = \begin{bmatrix} I & 0 & 0 & 0 & 0 \\ 0 & I & 0 & 0 & 0 \\ 0 & 0 & \alpha_f I & I & 0 \\ 0 & 0 & -\alpha_s I & I & 0 \\ 0 & 0 & 0 & 0 & I \end{bmatrix}, \tag{23}$$

where I stands for the identity matrices for the unknown arrays. We point out that these identity matrices have different dimensions but are not distinguished for the sake of simplicity. The residual in this case is a combination of (21) and (22)

$$\mathbf{r}^{k+1} = \alpha_f\mathbf{r}_D^{k+1} + \mathbf{r}_N^{k+1}.$$

From (23) we can easily obtain the different methods of Table 1 using the appropriate values of α_f and α_s.

5. Analysis of a model problem

In this section we analyze the convergence of the Robin–Dirichlet and Robin–Neumann iterative procedures and compare them with the more traditional Dirichlet–Neumann algorithm. In order to simplify the analysis, we consider the meaningful fluid–structure interaction (FSI) test problem suggested in [3] for the analysis of Dirichlet–Neumann and Neumann–Dirichlet algorithms, based on the simplified fluid model reported in Section 3.2. In particular, we consider a FSI system in which the fluid problem is two-dimensional and the structure problem one-dimensional. For the structure we consider the *generalized string model* and the *independent rings model* (see e.g. [19,16]). This test problem is a fair approximation of a blood-vessel system. The geometrical definition and notations are the same as in [3]. In particular, referring to Fig. 1, the fluid domain Ω_f is a rectangle and Σ is the part of its boundary on which the structure is located. The continuous fluid–structure problem consists of: find $\boldsymbol{u}$, p and η such that

$$\rho_f \partial_t \boldsymbol{u} + \nabla p = \boldsymbol{0} \quad \text{in } \Omega_f \times (0, T), \tag{24a}$$

$$\nabla \cdot \boldsymbol{u} = 0 \quad \text{in } \Omega_f \times (0, T), \tag{24b}$$

$$p = \bar{p} \quad \text{on } \Gamma^1 \cup \Gamma^2 \times (0, T), \tag{24c}$$

$$u = 0 \quad \text{on } \Gamma^3 \times (0, T), \tag{24d}$$

$$u = \partial_t \eta \quad \text{on } \Sigma \times (0, T), \tag{24e}$$

$$\rho_s H_s \partial_{tt} \eta + \beta \eta - b \partial_{xx} \eta = p \quad \text{on } \Sigma \times (0, T). \tag{24f}$$

Again, η denotes the structure displacement in the direction $\boldsymbol{n}_f$ and $u = \boldsymbol{u} \cdot \boldsymbol{n}_f$. Eq. (24e) imposes the *continuity of velocities* on the fluid–structure interface while the structure equation (24f) enforces the *continuity of stresses*. The rest of boundary conditions on the fluid domain boundary are: zero normal flux on Γ^3 and Neumann-type boundary conditions on the inflow and outflow sections, where a pressure $\bar{p}$ is imposed. We consider $\bar{p} = \bar{p}(x, y, t)$ possibly depending on space and time. Finally, system (24) is equipped with suitable initial conditions as well as homogeneous Dirichlet boundary conditions on η, whenever $b \neq 0$.

We consider the linear FSI system (24) since it is simple enough to be analyzed theoretically. On the other hand, it features a behavior similar to the more complex system (3). In particular, the structure model considered here is based on the simplified structure model proposed in Section 3.1, to which we have added a term involving space derivatives to approximate the elasticity operator in the tangential direction. We expect that the theoretical results obtained with this model give insightful information also for system (3).

We introduce now the time discrete version of system (24). Backward difference schemes are considered for the time integration of both fluid and structure equations. The discretized in time FSI problem at time step $n + 1$ reads as follows: given η^n and $\boldsymbol{u}^n$, find $\eta^{n+1}, \boldsymbol{u}^{n+1}$ and p^{n+1} such that

$$\rho_f \delta_t \boldsymbol{u}^{n+1} + \nabla p^{n+1} = \boldsymbol{0} \quad \text{in } \Omega_f, \tag{25a}$$

$$\nabla \cdot \boldsymbol{u}^{n+1} = 0 \quad \text{in } \Omega_f, \tag{25b}$$

$$p^{n+1} = \bar{p}^{n+1} \quad \text{on } \Gamma^1 \cup \Gamma^2, \tag{25c}$$

$$u^{n+1} = 0 \quad \text{on } \Gamma^3, \tag{25d}$$

$$u^{n+1} = \delta_t \eta^{n+1} \quad \text{on } \Sigma, \tag{25e}$$

$$\rho_s H_s \delta_{tt} \eta^{n+1} + \beta \eta^{n+1} - b \partial_{xx} \eta^{n+1} = p^{n+1} \quad \text{on } \Sigma. \tag{25f}$$
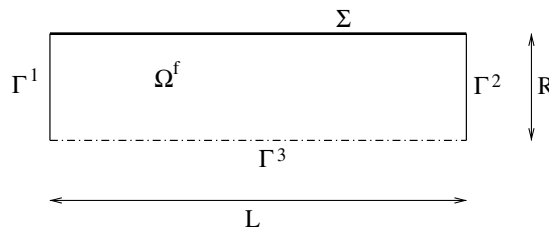

Fig. 1. Reference domains Ω_f.

Assuming that the solution is regular enough, the fluid problem (25a)–(25e) can be reformulated only in terms of the pressure, obtaining the following Poisson problem:

$$-\Delta p^{n+1} = 0 \quad \text{in } \Omega^f, \tag{26a}$$

$$p^{n+1} = \bar{p}^{n+1} \quad \text{on } \Gamma^1 \cup \Gamma^2, \tag{26b}$$

$$\frac{\partial p^{n+1}}{\partial \boldsymbol{n}} = 0 \quad \text{on } \Gamma^3, \tag{26c}$$

$$\frac{\partial p^{n+1}}{\partial \boldsymbol{n}} = -\rho_f \delta_t u^{n+1} \quad \text{on } \Sigma. \tag{26d}$$

Let us introduce the solution $\hat{p}^{n+1}$ of the problem

$$-\Delta \hat{p}^{n+1} = 0 \quad \text{in } \Omega^f, \tag{27a}$$

$$\hat{p}^{n+1} = \bar{p}^{n+1} \quad \text{on } \Gamma^1 \cup \Gamma^2, \tag{27b}$$

$$\frac{\partial \hat{p}^{n+1}}{\partial \boldsymbol{n}} = 0 \quad \text{on } \Gamma^3, \tag{27c}$$

$$\frac{\partial \hat{p}^{n+1}}{\partial \boldsymbol{n}} = 0 \quad \text{on } \Sigma \tag{27d}$$

and the *added-mass* operator

$$\mathcal{M} : H^{-1/2}(\Sigma) \to H^{1/2}(\Sigma),$$

$$\gamma \mapsto q|_\Sigma,$$

which consists of given $\gamma \in H^{-1/2}(\Sigma)$, find $q \in H^1(\Omega^f)$ such that

$$-\Delta q = 0 \quad \text{in } \Omega^f, \tag{28a}$$

$$q = 0 \quad \text{on } \Gamma^1 \cup \Gamma^2, \tag{28b}$$

$$\frac{\partial q}{\partial \boldsymbol{n}} = 0 \quad \text{on } \Gamma^3, \tag{28c}$$

$$\frac{\partial q}{\partial \boldsymbol{n}} = \gamma \quad \text{on } \Sigma \tag{28d}$$

and extract the value of the solution q on Σ. It can be proved that $\mathcal{M}(\cdot)$ is a self-adjoint operator on $L^2(\Sigma)$ (see [3]). Then, the pressure p^{n+1} solution of (26) on the interface Σ is given by

$$p^{n+1} = \hat{p}^{n+1} - \rho_f \mathcal{M}(\delta_t u^{n+1}) \quad \text{on } \Sigma. \tag{29}$$

This relation holds for any $(\boldsymbol{u}^{n+1}, p^{n+1})$ satisfying (25a)–(25e), independently of the type of boundary condition taken on Σ for the fluid problem. Therefore, (29) holds for all the partitioned algorithms considered in this section.

In what follows, we will consider the Dirichlet–Neumann, the Robin–Dirichlet and the Robin–Neumann algorithms. We will show that all of them can be written as fixed point algorithms on the variable η^{n+1}. We will also investigate the convergence rates of such algorithms according to the following definition:

Definition 1. Let η^{n+1} be the exact solution of the monolithic problem (25) and $\eta^{n+1,k}$ the kth iterate of the fixed point algorithm corresponding to either DN, RD or RN algorithm. Given a relaxation parameter ω, we define the asymptotic converge factor $\sigma(\omega)$ as the smallest positive number for which

$$\|\eta^{n+1,k+1} - \eta^{n+1}\|_{L^2(\Sigma)} \leqslant \sigma(\omega) \|\eta^{n+1,k} - \eta^{n+1}\|_{L^2(\Sigma)}$$

holds for any possible solution η^{n+1}.

From now on, for the sake of clarity, we omit the temporal index $n + 1$, that will be understood.

To analyze the fixed point algorithms we will decompose η on the L^2 orthonormal basis $\left\{ g_i(x) = \sqrt{\frac{2}{L}} \sin(\frac{i\pi x}{L}) \right\}_{i=1}^{\infty}$, that is

$$\eta = \sum_{i=1}^{\infty} \eta_i g_i. \tag{30}$$

Observe that the functions g_i are both eigenfunctions of the added-mass operator (see [3]) with corresponding eigenvalues

$$\mu_i = \frac{L}{i\pi \tanh\left(\frac{i\pi R}{L}\right)}, \quad i = 1, \ldots, \infty, \tag{31}$$

and eigenfunctions of the Laplace operator $\mathcal{L} = -\partial_{xx}$ on Σ, with corresponding eigenvalues

$$\lambda_i = \left(\frac{i\pi}{L}\right)^2.$$

In particular, we point out that the values λ_i increase with i and $\lambda_i \to \infty$ when $i \to \infty$, whereas the values μ_i decrese with i and $\mu_i \to 0$ when $i \to \infty$.

As we will show, for all three algorithms, the Fourier coefficients η_i satisfy the fixed point equation

$$\eta_i^{k+1} = (1 - \omega\gamma_i)\eta_i^k + f(\hat{p}, \eta^n, \eta^{n-1}, \boldsymbol{u}^n), \quad i = 1, \ldots, \infty \tag{32}$$

for a suitable f and $\gamma_i > 0$. Hence, the following resut that applies for a general Richardson algorithm (see e.g. [18]) can be used:

Lemma 1. *For those algorithms that can be written in form* (32), *we have*

(1) *the algorithm converges for*

$$0 < \omega < \frac{2}{\sup_i \gamma_i};$$

(2) *there exists an optimal choice*

$$\omega_{\text{opt}} = \frac{2}{\sup_i \gamma_i + \inf_i \gamma_i}$$

such that

$$\sigma_{\text{opt}} = \sigma(\omega_{\text{opt}}) = \frac{\sup_i \gamma_i - \inf_i \gamma_i}{\sup_i \gamma_i + \inf_i \gamma_i}$$

is minimal.

5.1. The Robin–Dirichlet algorithm

We begin by analyzing the Robin–Dirichlet algorithm for the proposed simplified problem. A Robin boundary condition for the fluid problem on Σ can be easily obtained applying $\rho_s H_s \delta_t(\cdot)$ to (25e) and substituting the result in (25f). Then, (25e) is replaced by

$$-\rho_s H_s \delta_t u + p = \beta\eta - b\partial_{xx}\eta \quad \text{on } \Sigma,$$

which can be written equivalently as

$$(\beta\Delta t^2 + \rho_s H_s)\delta_t u - p = -\beta\eta^n + b\partial_{xx}\eta - \beta\Delta t u^n \quad \text{on } \Sigma.$$

Observe that this condition is consistent with the general Robin condition $(7)_a$ with the choice $\alpha_f = \rho_s H_s/\Delta t + \beta\Delta t$. At this point, we can define the Robin–Dirichlet algorithm supplemented with a *relaxation technique*. For time step $n + 1$ and iteration $k + 1$ with $k > 0$, the method consists of given η^n, $\boldsymbol{u}^n$ and η^k, find η^{k+1}, $\boldsymbol{u}^{k+1}$ and p^{k+1} such that,

1. Fluid problem (Robin boundary condition)

$$\rho_f \delta_t \boldsymbol{u}^{k+1} + \nabla p^{k+1} = \boldsymbol{0}, \quad \text{in } \Omega_f, \tag{33a}$$

$$\nabla \cdot \boldsymbol{u}^{k+1} = 0 \quad \text{in } \Omega_f, \tag{33b}$$

$$p^{k+1} = \bar{p} \quad \text{on } \Gamma^1 \cup \Gamma^2, \tag{33c}$$

$$u^{k+1} = 0 \quad \text{on } \Gamma^3, \tag{33d}$$

$$(\beta \Delta t^2 + \rho_s H_s) \delta_t u^{k+1} - p^{k+1} = -\beta \eta^n + b \partial_{xx} \eta^k - \beta \Delta t u^n \quad \text{on } \Sigma. \tag{33e}$$

2. Structure problem (Dirichlet boundary condition)

$$\widetilde{\eta}^{k+1} = \Delta t u^{k+1} + \eta^n \quad \text{on } \Sigma. \tag{33f}$$

3. Relaxation step

$$\eta^{k+1} = \omega \widetilde{\eta}^{k+1} + (1 - \omega) \eta^k. \tag{33g}$$

The relaxation parameter ω might be necessary to guarantee convergence of the method. We observe that for this simple case the structural equation is never explicitly solved. This is due to the fact that the structure problem is a $d - 1$-dimensional manifold coupled via a Dirichlet boundary condition to the fluid. We point out that the algorithm given by (33) coincides with the Robin-based scheme proposed in [16]. In the next theorem we analyze the convergence properties of system (33).

Theorem 1. *The Robin–Dirichlet iterative algorithm* (33) *applied to the FSI test problem* (25) *never converges to the monolithic solution, when $b \neq 0$, for any choice of $\omega > 0$. Indeed, we have $\omega_{\text{opt}} = 0$ and $\sigma_{\text{opt}} = 1$. On the other hand, when $b = 0$, the algorithm converges in just one iteration.*

Proof. Substituting (29) in (33e) and thanks to (33f), we obtain

$$-\rho_f \mathcal{M}(\delta_{tt} \widetilde{\eta}^{k+1}) + \hat{p} = (\beta \Delta t^2 + \rho_s H_s) \delta_{tt} \widetilde{\eta}^{k+1} - b \partial_{xx} \eta^k + \beta \eta^n + \beta \Delta t u^n.$$

Due to the orthogonality of the basis $\{g_j\}_{j=0}^{\infty}$, by multiplying the latter equality by g_i and integrating over Σ, we obtain

$$(\rho_f \mu_i + \beta \Delta t^2 + \rho_s H_s) \delta_{tt} \widetilde{\eta}_i^{k+1} = -b \lambda_i \eta_i^k + \hat{p} - \beta \eta_i^n - \beta \Delta t u_i^n.$$

The previous equation together with (33g) leads to

$$\frac{1}{\omega} (\rho_s H_s + \rho_f \mu_i + \beta \Delta t^2) \eta_i^{k+1} = \left(\frac{1 - \omega}{\omega} (\rho_s H_s + \rho_f \mu_i + \beta \Delta t^2) - b \lambda_i \Delta t^2 \right) \eta_i^k + f(\hat{p}_i, \eta_i^n, \eta_i^{n-1}, u_i^n)$$

for a suitable f. We have then,

$$\eta_i^{k+1} = \left(1 - \omega \left(1 + \frac{b \lambda_i \Delta t^2}{\rho_s H_s + \rho_f \mu_i + \beta \Delta t^2} \right) \right) \eta_i^k + f(\hat{p}_i, \eta_i^n, \eta_i^{n-1}, u_i^n)$$

and therefore we obtain (32) with

$$\gamma_i = 1 + \frac{b \lambda_i \Delta t^2}{\rho_s H_s + \rho_f \mu_i + \beta \Delta t^2}. \tag{34}$$

By noticing that the function γ_i increases with i, we have, for $b \neq 0$,

$$\inf_i \gamma_i = \gamma_{\text{min}} = 1 + \frac{b \lambda_{\text{min}} \Delta t^2}{\rho_s H_s + \rho_f \mu_{\text{max}} + \beta \Delta t^2},$$

$$\sup_i \gamma_i = 1 + \frac{b \sup_i \lambda_i \Delta t^2}{\rho_s H_s + \rho_f \inf_i \mu_i + \beta \Delta t^2} = +\infty.$$

Therefore owing to Lemma 1, we can state that the algorithm never converges.

Otherwise, if $b = 0$, that is for the independent rings model, from (34) we obtain $\gamma_i \equiv 0$ and therefore, from Lemma 1, $\omega_{\mathrm{opt}} = 1$ and $\sigma_{\mathrm{opt}} = 0$. This means that in this case RD scheme converges in exactly 1 iteration. This is not surprising, since for $b = 0$ the RD algorithm coincides with the monolithic problem (see [16]). $\quad\square$

Remark 2. When considering discrete versions of the operators $\mathcal{M}$ and $\mathcal{L}$, for instance by means of a finite elements discretization, we expect the discrete eigenvalues $\hat{\lambda}_i, \hat{\mu}_i$ to behave as

$$\hat{\lambda}_{\max} = C_1 h^{-2}, \quad \hat{\mu}_{\min} = C_2 h, \tag{35}$$

where h is the space discretization parameter on Σ. Therefore, we expect that

$$\hat{\gamma}_{\min} \simeq 1 + \frac{b\hat{\lambda}_{\min}\Delta t^2}{\rho_s H_s + \rho_f \hat{\mu}_{\max} + \beta\Delta t^2},$$

$$\hat{\gamma}_{\max} \simeq 1 + \frac{b\hat{\lambda}_{\max}\Delta t^2}{\rho_s H_s + \rho_f \hat{\mu}_{\min} + \beta\Delta t^2}$$

obtaining, from Lemma 1 and owing to (35), that convergence should be reached for

$$0 < \hat{\omega} \lesssim \frac{2(\rho_s H_s + C_2 \rho_f h + \beta\Delta t^2)}{\rho_s H_s + C_2 \rho_f h + \beta\Delta t^2 + C_1 b\Delta t^2 h^{-2}}.$$

Moreover, the best convergence rate is

$$\hat{\sigma}_{\mathrm{opt}} \simeq \frac{\frac{C_1 b\Delta t^2 h^{-2}}{\rho_s H_s + C_2 \rho_f h + \beta\Delta t^2} - \frac{\hat{\lambda}_{\min} b\Delta t^2}{\rho_s H_s + \hat{\mu}_{\max}\rho_f + \beta\Delta t^2}}{2 + \frac{C_1 b\Delta t^2 h^{-2}}{\rho_s H_s + C_2 \rho_f h + \beta\Delta t^2} + \frac{\hat{\lambda}_{\min} b\Delta t^2}{\rho_s H_s + \hat{\mu}_{\max}\rho_f + \beta\Delta t^2}}$$

and therefore $\hat{\sigma}_{\mathrm{opt}} < 1$, that is, in practical computations, convergence is always possible. In particular, if we satisfy a "CFL-like" condition $\Delta t \simeq kh$ and take the limit $\Delta t \to 0$, we observe that

$$\sigma_{\mathrm{opt}} \simeq \frac{C_1 kb}{2\rho_s H_s + C_1 kb}.$$

We expect, then, the convergence to be fast if $C_1 b \ll \rho_s H_s$ and slow when the elasticity term dominates over the inertial one. This result is expected since in the RD algorithm we treat explicitly the elastic term and implicitly the inertial term.

5.2. The Robin–Neumann algorithm

In this section we prove convergence results for the Robin–Neumann algorithm, the most promising of the partitioned procedures designed in this work. The only difference with respect to system (33) is in the structure step, which does involve the solution of the structural equation. As we will prove below, this fact has a dramatic impact on the convergence properties of the algorithm (with respect to the Robin–Dirichlet method). For time step $n + 1$ and iteration $k + 1$ with $k > 0$, the Robin–Neumann method consists of: given $\eta^n, \boldsymbol{u}^n$ and η^k, find $\eta^{k+1}, \boldsymbol{u}^{k+1}$ and p^{k+1} such that,

1. Fluid problem (33a)–(33e) (Robin boundary condition)
2. Structure problem (Neumann boundary condition)

$$\rho_s H_s \delta_{tt}\tilde{\eta}^{k+1} + \beta\tilde{\eta}^{k+1} - b\partial_{xx}\tilde{\eta}^{k+1} = p^{k+1} \quad \text{on } \Sigma. \tag{36}$$

3. Relaxation step (33g).

The next theorem is devoted to the stability properties of this method.

Theorem 2. *The Robin–Neumann iterative algorithm* (33a)–(33e), (36), (33g) *applied to the FSI test problem* (25) *em converges to the monolithic solution under the following condition for the relaxation parameter:*

$$0 < \omega < 2. \tag{37}$$

Moreover, the convergence rate for $\omega = 1$ is given by

$$\sigma(1) = \frac{1}{1 + \left(\frac{\beta \Delta t^2 + \rho_s H_s}{\rho_f \mu_{\bar{i}}} + \frac{\beta \Delta t^2 + \rho_s H_s}{b \lambda_{\bar{i}} \Delta t^2} + \frac{(\beta \Delta t^2 + \rho_s H_s)^2}{b \rho_f \mu_{\bar{i}} \lambda_{\bar{i}} \Delta t^2} \right)}, \tag{38}$$

whereas the best convergence rate is characterized by

$$\sigma_{\mathrm{opt}} = \frac{1}{1 + 2 \left(\frac{\beta \Delta t^2 + \rho_s H_s}{\rho_f \mu_i} + \frac{\beta \Delta t^2 + \rho_s H_s}{b \lambda_{\bar{i}} \Delta t^2} + \frac{(\beta \Delta t^2 + \rho_s H_s)^2}{b \rho_f \mu_i \lambda_{\bar{i}} \Delta t^2} \right)} \tag{39}$$

for a suitable index $\bar{i} = \mathrm{argmin} \left(1 + \frac{\beta \Delta t^2 + \rho_s H_s}{\rho_f \mu_i} \right) \left(1 + \frac{\beta \Delta t^2 + \rho_s Hs}{b \lambda_i \Delta t^2} \right).$

Proof. This result can be proved following the same lines as in the previous theorem. From (29), we know that

$$\mathcal{M}^{-1}(p^{k+1} - \hat{p}) = -\rho_f \delta_t u^{k+1}.$$

Invoking this equality in (33e) we get

$$\left(\frac{\beta \Delta t^2 + \rho_s H_s}{\rho_f} \mathcal{M}^{-1} + I \right) p^{k+1} = -b \partial_{xx} \eta^k + f(\hat{p}, \eta^n, \boldsymbol{u}^n) \tag{40}$$

for a suitable f and where I is the identity operator. On the other hand, the value of p^{k+1} is determined by (36):

$$p^{k+1} = \rho_s H_s \delta_{tt} \widetilde{\eta}^{k+1} + \beta \widetilde{\eta}^{k+1} - b \partial_{xx} \widetilde{\eta}^{k+1}. \tag{41}$$

Combining (40) and (41), we obtain

$$\left(\frac{\beta \Delta t^2 + \rho_s H_s}{\rho_f} \mathcal{M}^{-1} + I \right) \left(\rho_s H_s \delta_{tt} \widetilde{\eta}^{k+1} + \beta \widetilde{\eta}^{k+1} - b \partial_{xx} \widetilde{\eta}^{k+1} \right) = -b \partial_{xx} \eta^k + f(\hat{p}, \eta^n, \boldsymbol{u}^n). \tag{42}$$

As above, we can use the decomposition (30) and write the previous equation for every component η_i^{k+1}. Let us define the following value:

$$\psi_i = \left(\frac{\beta \Delta t^2 + \rho_s H_s}{\rho_f \mu_i} + 1 \right) \left(\frac{\rho_s H_s}{\Delta t^2} + \beta + b \lambda_i \right).$$

It allows us to write (42) in form (32) with

$$\gamma_i = 1 - \frac{b \lambda_i}{\psi_i}.$$

We observe that $0 < \gamma_i \leqslant 1$ and it is not monotone in general. In particular, it reaches its maximum for $i \to \infty$ (where $\gamma_i \to 1$) and its minimum for a suitable index $\bar{i}$ depending on the parameters of the problem. Then, owing to Lemma 1 and rearranging, we obtain (37) and (39). Moreover, if $\omega = 1$, from (32) we obtain $\sigma(1) = \max_i |1 - \gamma_i| = 1 - \gamma_{\bar{i}}$, leading to (38). $\square$

Remark 3. When $b = 0$ the RN scheme coincides with the monolithic problem. Indeed, from (39) it follows that $\omega_{\mathrm{opt}} = 1$ and $\sigma_{\mathrm{opt}} = 0$ and then RN converges in just one iteration. On the other hand, when $b \neq 0$ and $\Delta t \to 0$, the convergence gets faster and faster.

From (39), we observe that the convergence rate gets worse if the ratio ρ_s/ρ_f decreases or if the elastic term b increases. However, due to the presence of three terms in the bracket in (39), the value of σ_{opt} is in any case far from 1, and therefore it seems that the RN scheme is not too sensible to the variation of b and to the added-mass effect, as the numerical results in Section 6 confirm. The same considerations holds when using $\omega = 1$, since $\sigma(1)$ exhibits the same dependence on the parameters.

5.3. The Dirichlet–Neumann algorithm

In this section, we extend the results shown in [3], concerning the convergence of the DN algorithm, to the generalized string model. Moreover, we provide also for this scheme the optimal values of the asymptotic converge factor. In particular, we have the following

Theorem 3. *The Dirichlet–Neumann iterative algorithm applied to the FSI test problem* (25) *converges to the monolithic solution under the following condition on the relaxation parameter*:

$$0 < \omega \leqslant \frac{2}{1 + \frac{\mu_{\max}\rho_f}{\rho_s H_s + \beta\Delta t^2 + \lambda_{\min}b\Delta t^2}}. \tag{43}$$

Moreover, *the best convergence rate is characterized by*

$$\sigma_{\mathrm{opt}} = \frac{1}{1 + 2\frac{\rho_s H_s + \beta\Delta t^2 + b\lambda_{\min}\Delta t^2}{\mu_{\max}\rho_f}}. \tag{44}$$

Proof. In this case we can write the algorithm in form (32) with

$$\gamma_i = 1 + \frac{\rho_f \mu_i}{\rho_s H_s + \beta\Delta t^2 + b\Delta t^2\lambda_i}.$$

By noticing that the function γ_i decreases with i, owing to Lemma 1 we obtain (43) and (44). $\quad\square$

From (44), we observe that the convergence rate gets worse if b decreases. Moreover, it depends heavily on the ratio ρ_s/ρ_f, that is the DN scheme is very sensible to the added-mass effect, as already pointed out in [3] and as the numerical results confirm.

6. Numerical results

In this section we present some numerical results with the aim of testing the algorithms proposed in the previous sections. As pointed out in Section 2.1, we call semi-implicit the algorithms in which we do not update in the loop neither the convective term nor the fluid domain, otherwise we refer to them as implicit. In particular, in Section 6.1 we test the performance of the semi-implicit Robin–Dirichlet (SIRD) and Robin–Neumann (SIRN) algorithms, in comparison with the semi-implicit Dirichlet–Neumann scheme (EDN). Moreover, we test the implicit Robin–Neumann algorithm (IRN). In Section 6.2 we detail the performance of the semi-implicit Robin–Robin, Dirichlet–Robin and Neumann–Robin algorithms.

For the structure, we consider the following equation of linear elasticity:

$$\rho_s\partial_{tt}\boldsymbol{\eta} - c\nabla\cdot(\nabla\boldsymbol{\eta} + (\nabla\boldsymbol{\eta})^t) - \lambda\nabla\cdot((\nabla\cdot\boldsymbol{\eta})I) + \beta\boldsymbol{\eta} = \boldsymbol{f}_s,$$

where I is the identity operator, $c = E/(1 + v)$, and $\lambda = vE/((1 + v)(1 - 2v))$. The reaction terms stand for the transversal membrane effects that appear when the structure is written in axisymmetric form.

All the numerical simulations are performed in a rectangular domain both for the fluid and for the two structures, whose size is 6×1 cm and 6×0.1 cm, respectively (see Fig. 2). We use a 2D Finite Element Code
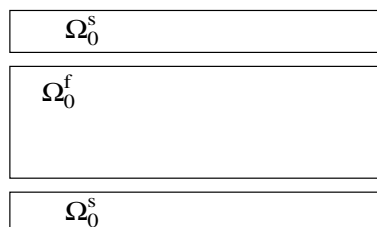

Fig. 2. Computational fluid and structure domains.

written in Matlab at MOX-Dipartimento di Matematica-Politecnico di Milano and at CMCS-EPFL-Lausanne. Moreover, we consider $\mathbb{P}_1 iso \mathbb{P}_2$ and $\mathbb{P}_1$ elements for the fluid and $\mathbb{P}_1$ element for the structure and a space discretization step $h = 0.02$ cm. In all the cases we use the residual normalized on the initial one as stopping criterion (see Section 4), with a tolerance equal to 10^{-4}.

We set $\mu = 0.035$ poise, $\rho_f = 1$ g/cm^3 and, unless otherwise specified, we consider the following other values: $\Delta t = 10^{-3}$ s, $\rho_s = 1.1$ g/cm^3, $c = 1.15 \times 10^6$ dyne/cm^2, $\lambda = 1.7 \times 10^6$ dyne/cm^2, $\beta = 4 \times 10^6$ dyne/cm^4 and the thickness of the structure $H_s = 0.1$ cm.

6.1. The Robin–Neumann and the Robin–Dirichlet schemes

In this section we study the performance of the Robin–Neumann and the Robin–Dirichlet schemes. When we prescribe a Robin boundary condition for the fluid, an optimal choice for the parameter α_f, as (12) suggests, is naturally given by the simplified model for the structure equation, that is $\alpha_f = H_s \rho_s / \Delta t + \beta \Delta t$. This value is directly computable, hence very useful in practical computations.

Let us start with the semi-implicit case. In Fig. 3 we show the solution computed with the SIRN scheme, which, of course, is the same as the one computed with the semi-implicit monolithic scheme (SIM), up to the employed tolerance. In particular, this figure shows average quantities on a radial section of the mean pressure (top), the flow rate (middle), and the fluid domain radius (bottom), as a function of the axial coordinate.

Fig. 4 shows the structure displacement, obtained with the SIRN scheme, in the deformed domain at three different instants. In Table 2 we show the average number of iterations in the first 12 time steps, employed by the SIRN, SIRD and SIDN schemes, in three cases: without relaxation ($\omega = 1$), with an optimally tuned relaxation parameter (ω_{opt}) and using an Aitken relaxation procedure (see [14,4]). First of all, we point out that SIRN is the only algorithm that converges without relaxation. This is a very interesting feature of this scheme. Moreover, SIRN is always much faster than SIDN. This is confirmed also by Fig. 5 that plots the errors on several quantities, measured in the L^∞ norm, versus the number of iterations. To compute the errors, we have taken as reference solution the one provided by the SIM scheme. In all these tests, we have employed an optimal relaxation parameter. On the other hand, the SIRD scheme is very slow and the relative error at convergence is high, evidencing high condition number of this problem. However, as Table 3 shows, the

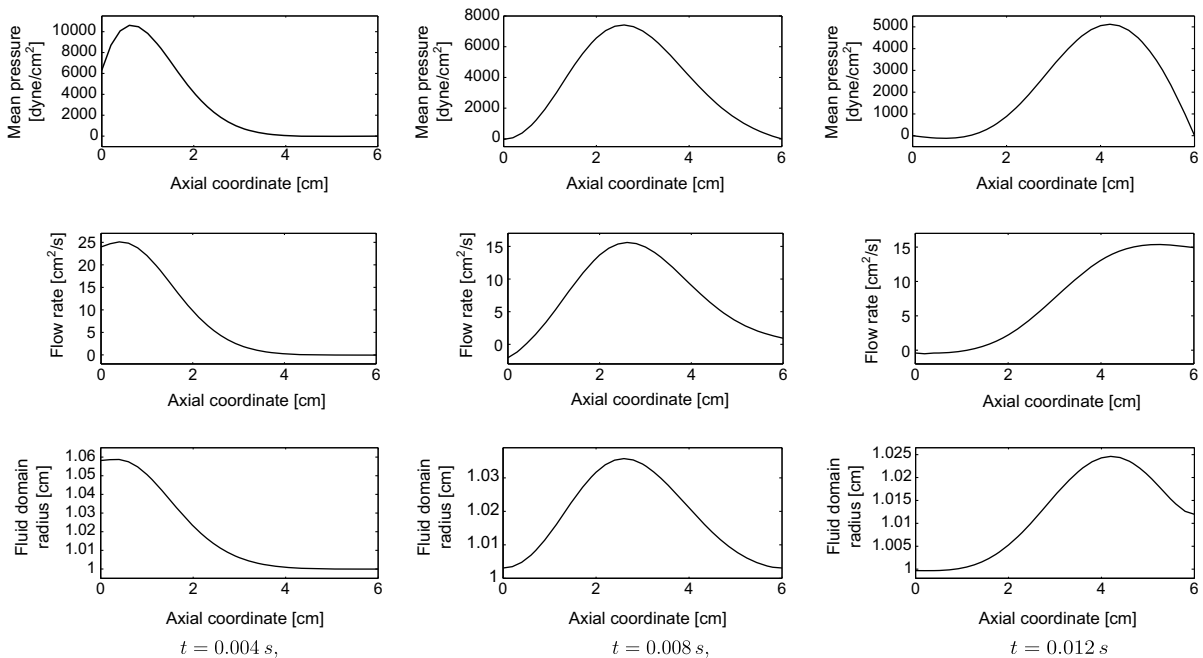$t = 0.004\ s,$ $\qquad\qquad\qquad\qquad$ $t = 0.008\ s,$ $\qquad\qquad\qquad\qquad$ $t = 0.012\ s$

Fig. 3. SIRN scheme. Mean pressure (top), flow rate (middle) and fluid domain radius (bottom) at three time instants.
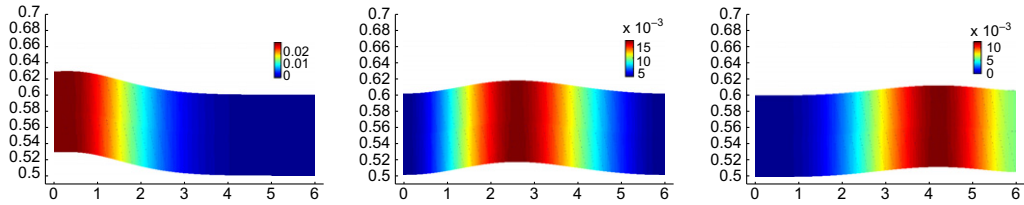
Fig. 4. Displacement of the structure-SIRN scheme-$t = 0.004$ s (left), $t = 0.008$ s (middle) and at $t = 0.012$ s (right).

Table 2
Average number of iterations per time step for the three schemes without relaxation ($\omega = 1$), with an optimal choice of the relaxation parameter (ω_{opt}) and using an Aitken procedure

	SIDN	SIRN	SIRD
$\omega = 1$	NO	7.00	NO
ω_{opt}	73.25 (0.09)	7.00 (1)	394.00 (0.015)
Aitken	15.50	6.00	123.75

In brackets, the value of the optimal parameter.

number of iterations decreases if we consider a small value of the elastic coefficients, as expected from the analysis of Section 5. Due to its inefficiency, from now on we drop the Robin–Dirichlet scheme and we focus on the Robin–Neumann algorithm only.

In the sequel, we compare the SIDN and SIRN performance, studying their sensitivity with respect to some of the parameters of the fluid and structure models; see Table 3. First of all, we point out that SIRN always converges without relaxation, while SIDN always needs a relaxation parameter smaller than one. Moreover, SIRN shows a number of iterations quite insensitive to the values of physical and numerical parameters and 5–20 times less than SIDN. In particular, we observe that the convergence of SIDN is deteriorated when the added-mass effect becomes more important, that is to say, the value ρ_s/ρ_f increases. On the contrary, SIRN is insensitive to this phenomenon. Changing the stiffness parameters c and λ, the two algorithms have different behaviours: SIDN seems to improve the convergence rate when these parameters increase, while SIRN when they decrease (even if in the last case the variation is very small). Finally, decreasing the time step Δt and the thickness H_s we observe that the convergence rate of SIDN gets worse, while for SIRN there is only a slight worsening. All these numerical simulations are consistent with the theoretical results presented in Section 5.

In conclusion, we can state that the *SIRN algorithm is clearly more robust and faster than the SIDN scheme*.

Let us consider now the implicit algorithms. In Fig. 6 we compare the mean pressure, the flow rate and the radius of the fluid domain obtained with the SIRN and IRN algorithms. We point out that IRN does not converge using the same iterative loop to update the convective term and the fluid domain, on one hand, and to solve the block Gauss–Seidel system, on the other one. Therefore, we need to use two nested loops: an external one in which we update the convective field and the fluid domain and an internal one in which we solve the block Gauss–Siedel system, as described in Remark 1. However, as numerical evidence suggests, it is sufficient to take $tol = 10^{-1}$ as tolerance for the internal loop. On the other hand, the implicit Dirichlet–Neumann scheme (IDN) converges using just one loop. Anyhow, as Table 4 shows, the average number of total sub-iterations N (that is the product of the internal and external sub-iterations) per time step is less for IRN, showing that also in the implicit case the Robin–Neumann partitioned procedure is faster than the Dirichlet–Neumann one. This is confirmed by Fig. 7 showing the L^∞ relative errors, using the implicit-monolithic (IM) algorithm as the reference solution and choosing optimally the relaxation parameter.

6.2. Schemes based on a Robin boundary condition for the structure

In this section we analyze the semi-implicit Robin–Robin (SIRR), Dirichlet–Robin (SIDR) and Neumann–Robin (SINR) schemes. Let us start with the semi-implicit Robin–Robin scheme. As pointed out in Sections
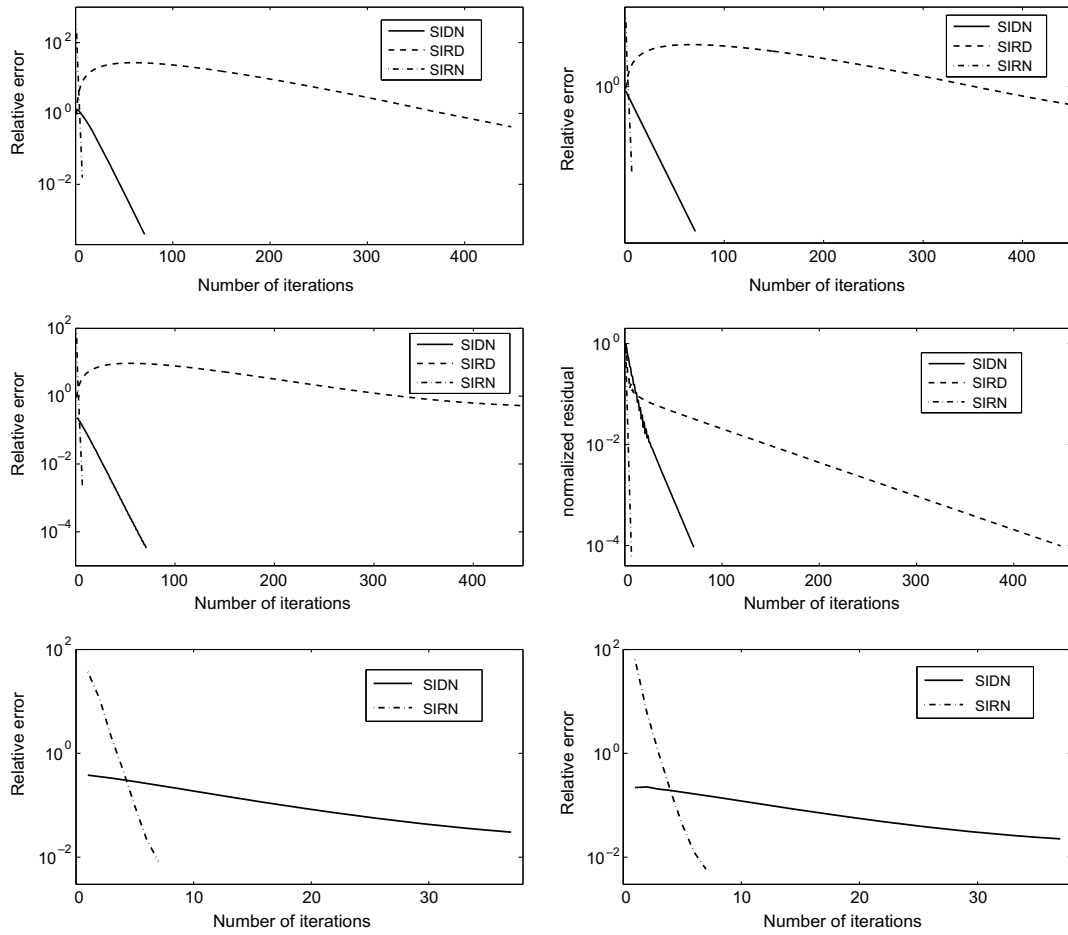
Fig. 5. Relative errors in L^∞ norm with optimal relaxation parameter. Top, left: fluid velocity error, $t = 0.004$ s. Top, right: pressure error, $t = 0.004$ s. Middle, left: structure displacement error, $t = 0.004$ s. Middle, right: residual normalized with the initial one, $t = 0.004$ s. Bottom, left: fluid velocity error, $t = 0.012$ s. Bottom, right: structure displacement error, $t = 0.012$ s.

Table 3
Average number of iterations per time step for SIDN and SIRN schemes, with an optimal choice of the relaxation parameter, varying the structure thickness H_s, the structure density ρ_s, the stiffness parameters c and λ and the time step Δt

	SIDN	SIRN	SIRD
Basic parameter	73.25 (0.09)	7.00 (1)	394.00 (0.015)
	186.25 (0.03)	9.00 (1.25)	
$H_s = 0.15$	32.00 (0.215)	5.50 (1)	
$\rho_s = 5$	36.50 (0.185)	5.75 (1.125)	
$\rho_s = 50$	14.00 (0.5)	4.00 (1)	
$5c, 5\lambda$	49.75 (0.125)	7.75 (1.25)	97.50 (0.075)
$c/5, \lambda/5$	76.25 (0.09)	5.50 (1)	
$\Delta t = 0.002$	27.25 (0.25)	5.50 (1)	
$\Delta t = 0.0005$	112.50 (0.05)	7.50 (1.25)	

In brackets, the value of the optimal parameter.

3.2 and 6.1, when we prescribe a Robin boundary condition for the fluid, an optimal choice for the parameter α_f is naturally given by the simplified model for the structure equation. On the other hand, when we prescribe a Robin boundary condition for the structure, we proposed in Section 3.1 a value of the parameter α_s depend-
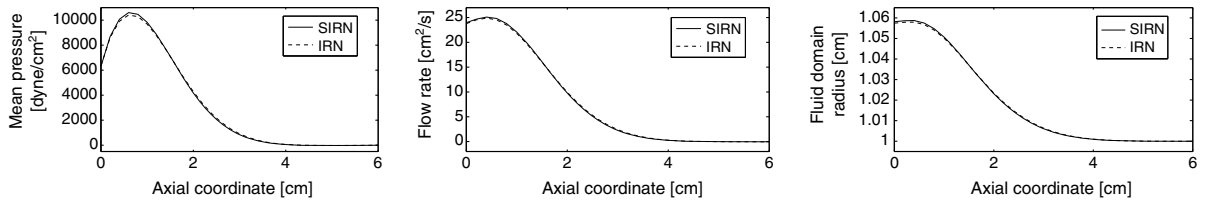
Fig. 6. Comparision between the SIRN and IRN solutions. Mean pressure (left), flow rate (middle) and fluid domain radius (right) – $t = 0.004$ s.

Table 4
Number of iterations N for IDN and IRN schemes, with an optimal choice of the relaxation parameter

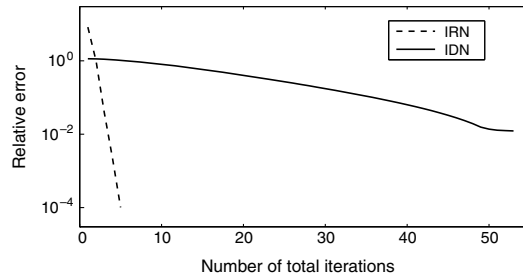|	IDN	IRN
ω_{opt}	0.09	1
N	61.75	14.25

Fig. 7. Relative errors in L^∞ norm with optimal relaxation parameter for IDN and IRN: fluid velocity error – $t = 0.004$ s.

Table 5
Average number of iterations per time step of the SIRR scheme for different values of the coefficient γ

γ	2×10^{-7}	2×10^{-5}	10^{-4}	0.005	0.01	0.02	0.05	1
Number of iteration	7.00	7.00	7.00	6.25	6.00	9.00	58.25	72.23

Table 6
Average number of iterations per time step of SIRR with $\gamma = 0.01$ and of SIRN

ρ_f	Δt	h	L	R	SIRR	SIRN
1.0	10^{-3}	0.2	6	0.5	6.00	7.00
1.0	5×10^{-4}	0.2	6	0.5	7.00	7.50
1.0	2×10^{-3}	0.2	6	0.5	5.00	5.50
1.0	10^{-3}	0.1	6	0.5	6.00	7.00
0.1	10^{-3}	0.2	6	0.5	6.75	7.00
1.0	10^{-3}	0.2	3	0.5	6.00	7.00
1.0	10^{-3}	0.2	6	0.25	7.00	8.00

In both cases the relaxation parameter is $\omega = 1$.

ing on a coefficient γ to be suitably chosen, namely $\alpha_s = \gamma \rho_f \mu_{max} / \Delta t$. Here, we study the sensitivity of the performance of the Robin–Robin scheme with respect to the values of γ, in terms of average number of iterations per time step. The results are given in Table 5. We point out that we have an optimal performance around the
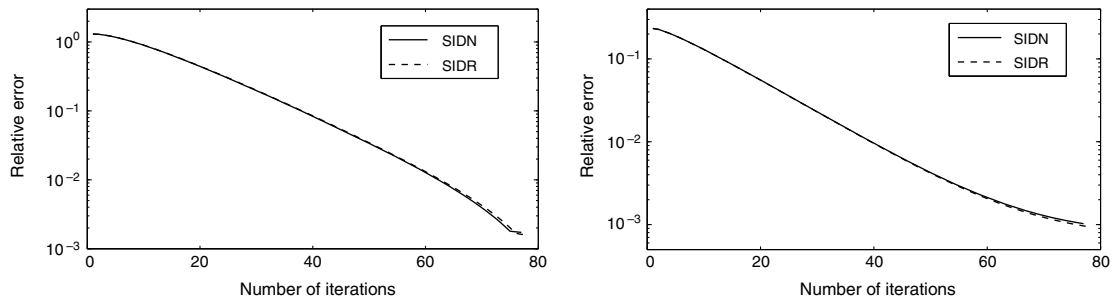
Fig. 8. Relative errors in L^∞ norm with optimal relaxation parameter. Left: fluid velocity error, right: structure displacement error – $t = 0.004$ s.

value $\gamma = 0.01$, which provides a convergence rate higher than the SIRN scheme. For values $\gamma < 0.005$ the behaviour is the same of the SIRN algorithm, while for values greater than 0.02 the convergence rate deteriorates. In Table 6, we show the number of iterations obtained with SIRN and with SIRR using the best coefficient γ found in the previous simulation for different values of $\rho_f, \Delta t, R, L$ and the characteristic mesh size h, that is for different parameters appearing in estimate (16). We observe that with this choice, the performance of SIRR is always better than SIRN and the value $\gamma = 0.01$ seems to be optimal also when changing the other parameters. The results given in Table 6 clearly show that this choice of γ is robust.

For what concerns the SIDR algorithm, the numerical results shows that for $\gamma < 0.02$ its performance is very close to the ones of SIDN scheme. In particular, for $\gamma = 0.01$ we obtain $\omega_{opt} = 0.09$ and 74.25 iterations (in average) to reach convergence. Moreover, Fig. 8 shows that the relative errors for SIDN and SIDR schemes are almost the same in this case. For values $\gamma > 0.02$ the performance of the SIDR scheme deteriorates as seen for the SIRR scheme.

Finally, we have experienced that the SINR algorithm does not converge.

7. Conclusions

The classical Dirichlet–Neumann algorithm is negatively affected by the added-mass effect. Therefore, for FSI applications where this effect is important, DN needs a strong relaxation and its convergence is very slow. We have obtained some new convergence results that are in accordance with this behavior.

The main contribution of this work is the design of *partitioned procedures suitable for FSI problems where the added-mass effect is important*, as, for instance, in hemodynamics applications. With this aim, we have introduced a new family of partitioned procedures generated by Robin transmission conditions, i.e. linear combination of Dirichlet (continuity of velocities) and Neumann (continuity of stresses) conditions on the interface. The convergence of the Robin-based algorithms depends on the choice of the combination coefficients. We have proposed those coefficients based on explicit formulae for simplified models for the fluid and for the structure.

In particular, we have analyzed two of these new methods: Robin–Dirichlet and Robin–Neumann. Whereas the Robin–Dirichlet algorithm is fairly disappointing, the Robin–Neumann algorithm does exhibit excellent convergence properties that make this algorithm very appealing:

- The method *always converges*, without any relaxation.
- The convergence is *insensitive to the added-mass effect*.

These properties have been proved theoretically for simplified blood-vessel system and checked for more general fluid and structure models using numerical experimentation. These two properties make the RN algorithm very useful in hemodynamics applications. In fact, this method converges much faster than DN for a wide set of numerical tests.

We have also proposed the more general RR scheme, that depends on the scaling factor γ. By suitably tuning this coefficient, we obtain convergence properties for the RR scheme even better than those of the RN

algorithm. Moreover, the tuned value seems to be very robust and practically independent of some of the parameters defining the problem at hand.

Even though we have not considered this point in this article, the use of a Robin transmission condition for the fluid system *allows to solve FSI problems with enclosed fluid domains* (balloon-type problems). The DN algorithm is useless in these cases because the fluid sub-problem is confined (Dirichlet boundary conditions on the whole fluid boundary). Furthermore, those Dirichlet boundary conditions for the fluid are obtained from the structure sub-problem and do not satisfy

$$\int_{\partial\Omega_f} \boldsymbol{u} \cdot \boldsymbol{n}_f = 0$$

in general. Thus, the null divergence constraint cannot be fulfilled, leading to unphysical results. The application of RN to this kind of problems will be the subject of a future work.

Acknowledgments

References

[1] S. Badia, A. Quaini, A. Quarteroni, Splitting methods based on algebraic factorization for fluid–structure interaction, SIAM J. Sci. Comput. 30 (4) (2008) 1778–1805.
[2] K.J. Bathe, H. Zhang, M.H. Wang, Finite element analysis of incompressible and compressible fluid flows with free surfaces and structural interactions, Comput. Struct. 56 (1995) 193–213.
[3] P. Causin, J.F. Gerbeau, F. Nobile, Added-mass effect in the design of partitioned algorithms for fluid–structure problems, Comput. Methods Appl. Mech. Eng. 194 (42–44) (2005) 4506–4527.
[4] S. Deparis. Numerical analysis of axisymmetric flows and methods for fluid–structure interaction arising in blood flow simulation, Ph.D. Thesis, École Polytechnique Fédérale de Lausanne, 2004.
[5] S. Deparis, M. Discacciati, G. Fourestey, A. Quarteroni, Fluid–structure algorithms based on Steklov–Poincaré operators, Comput. Methods Appl. Mech. Eng. 195 (41–43) (2006) 5797–5812.
[6] J. Donea, An arbitrary Lagrangian–Eulerian finite element method for transient dynamic fluid–structure interaction, Comput. Methods Appl. Mech. Eng. 33 (1982) 689–723.
[7] M.A. Fernández, J.F. Gerbeau, C. Grandmont, A projection semi-implicit scheme for the coupling of an elastic structure with an incompressible fluid, Int. J. Numer. Mech. Eng. 69 (4) (2007) 794–821.
[8] M.A. Fernández, M. Moubachir, A Newton method using exact Jacobians for solving fluid–structure coupling, Comput. Struct. 83 (2-3) (2005) 127–142.
[9] C. Figueroa, I. Vignon-Clementel, K. Jansen, T. Hughes, C. Taylor, A coupled momentum method for modeling blood flow in three-dimensional deformable arteries, Comput. Methods Appl. Mech. Eng. 195 (2006) 5685–5706.
[10] C. Forster, W. Wall, E. Ramm, Artificial added mass instabilities in sequential staggered coupling of nonlinear structures and incompressible viscous flow, Comput. Methods Appl. Mech. Eng. 196 (7) (2007) 1278–1293.
[11] J.F. Gerbeau, M. Vidrascu, A quasi-Newton algorithm based on a reduced model for fluid–structure interaction problems in blood flows, Math. Modell. Numer. Anal. 37 (4) (2003) 631–648.
[12] T.J.R. Hughes, W.K. Liu, T.K. Zimmermann, Lagrangian–Eulerian finite element formulation for incompressible viscous flows, Comput. Methods Appl. Mech. Eng. 29 (3) (1981) 329–349.
[13] H.G. Matthies, J. Steindorf, Partitioned but strongly coupled iteration schemes for nonlinear fluid–structure interaction, Comput. Struct. 80 (2002) 1991–1999.
[14] D.P. Mok, W.A. Wall, E. Ramm, Accelerated iterative substructuring schemes for instationary fluid–structure interaction, in: K.J. Bathe (Ed.), Computational Fluid and Solid Mechanics, Elsevier, 2001, pp. 1325–1328.
[15] F. Nobile, Numerical approximation of fluid–structure interaction problems with application to haemodynamics, Ph.D. Thesis, École Polytechnique Fédérale de Lausanne, 2001.
[16] F. Nobile, C. Vergara, An effective fluid–structure interaction formulation for vascular dynamics by generalized Robin conditions, SIAM J. Sci. Comput. 30 (2) (2008) 731–763.

[17] S. Piperno, C. Farhat, Design of efficient partitioned procedures for transient solution of aeroelastic problems, Rev. Eur. Elements Finis 9 (6-7) (2000) 655–680.

[18] A. Quarteroni, R. Sacco, F. Saleri, Numerical Mathematics, Springer, Berlin, 2000.

[19] A. Quarteroni, M. Tuveri, A. Veneziani, Computational vascular fluid dynamics: problems, models and methods, Comput. Visualisat. Sci. 2 (2000) 163–197.

[20] P. Le Tallec, J. Mouro, Fluid structure interaction with large structural displacements, Comput. Methods Appl. Mech. Eng. 190 (2001) 3039–3067.